Resource

Visualizing Spatiotemporal Dynamics of Multicellular Cell-Cycle Progression

Asako Sakaue-Sawano,[1,3] Hiroshi Kurokawa,[1,4] Toshifumi Morimura,[2] Aki Hanyu,[5] Hiroshi Hama,[1] Hatsuki Osawa,[1] Saori Kashiwagi,[2] Kiyoko Fukami,[4] Takaki Miyata,[6] Hiroyuki Miyoshi,[7] Takeshi Imamura,[5] Masaharu Ogawa,[2] Hisao Masai,[8] and Atsushi Miyawaki[1,3,*]

[1]Laboratory for Cell Function and Dynamics
[2]Laboratory for Cell Culture Development
Advanced Technology Development Group, Brain Science Institute, RIKEN, 2-1 Hirosawa, Wako-city, Saitama 351-0198, Japan
[3]Life Function and Dynamics, ERATO, JST, 2-1 Hirosawa, Wako-city, Saitama 351-0198, Japan
[4]School of Life Science, Tokyo University of Pharmacy and Life Science, 1432-1 Horinouchi, Hachioji, Tokyo 192-0392, Japan
[5]Departments of Biochemistry, The Cancer Institute of the Japanese Foundation for Cancer Research, 3-10-6 Ariake, Koto-ku, Tokyo 135-8550, Japan
[6]Department of Anatomy and Cell Biology, Nagoya University Graduate School of Medicine, 65 Tsurumai-cho, Syowa-ku, Nagoya, Aichi 466-8550, Japan
[7]Subteam for Manipulation of Cell Fate, BioResource Center, RIKEN Tsukuba Institute, 3-1-1 Koyadai, Tsukuba, Ibaraki 305-0074, Japan
[8]Genome Dynamics Project, Tokyo Metropolitan Institute of Medical Science, 3-18-22 Honkomagome, Bunkyo-ku, Tokyo 113-8613, Japan
*Correspondence: matsushi@brain.riken.jp
DOI 10.1016/j.cell.2007.12.033

SUMMARY

The cell-cycle transition from G_1 to S phase has been difficult to visualize. We have harnessed antiphase oscillating proteins that mark cell-cycle transitions in order to develop genetically encoded fluorescent probes for this purpose. These probes effectively label individual G_1 phase nuclei red and those in S/G_2/M phases green. We were able to generate cultured cells and transgenic mice constitutively expressing the cell-cycle probes, in which every cell nucleus exhibits either red or green fluorescence. We performed time-lapse imaging to explore the spatiotemporal patterns of cell-cycle dynamics during the epithelial-mesenchymal transition of cultured cells, the migration and differentiation of neural progenitors in brain slices, and the development of tumors across blood vessels in live mice. These mice and cell lines will serve as model systems permitting unprecedented spatial and temporal resolution to help us better understand how the cell cycle is coordinated with various biological events.

INTRODUCTION

Considerable progress has been made toward understanding the mechanism of cell-cycle progression in individual cells (Nurse et al., 1998; Nurse, 2000). However, the cell cycle is regulated not only by intracellular signals, but also by extracellular signals, and less is known about how the cell cycle is coordinated with differentiation, morphogenesis, and cell death in a multicellular context. While the transition from M to G_1 phase—namely cell division—can be monitored by morphological changes, the transition from G_1 to S is difficult to observe in live samples. To date, the G_1/S transition has mostly been observed either after nuclear bromodeoxyuridine (BrdU) staining, or by synchronizing the cell cycle by pharmacological means. Recently, several cell-cycle markers that identify the S phase and the subsequent transition to G_2 in live cells have been developed by fusing fluorescent proteins to proliferating cell nuclear antigen (PCNA) (Leonhardt et al., 2000; Essers et al., 2005; Kisielewska et al., 2005), DNA ligase I (Easwaran et al., 2005), or the C terminus of helicase B (GE healthcare). However, since identification of cell-cycle transitions requires the detection of subtle and often minute changes in the distribution pattern and intensity of fluorescence signals, these markers cannot track phase transitions with high contrast.

In addition to being regulated at the transcriptional and posttranslational levels, the cell cycle is controlled by ubiquitin (Ub)-mediated proteolysis (Figure 1A) (Ang and Harper, 2004; Nakayama and Nakayama, 2006). The APC^{Cdh1} and SCF^{Skp2} complexes are E3 ligase activities that mark a variety of proteins with Ub in a cell cycle-dependent manner (Vodermaier, 2004). Because the SCF^{Skp2} complex is a direct substrate of the APC^{Cdh1} complex but also functions as a feedback inhibitor of APC^{Cdh1} (Wei et al., 2004; Benmaamar and Pagano, 2005), these two ligase activities oscillate reciprocally during the cell cycle. The APC^{Cdh1} complex is active in the late M and G_1 phases, while the SCF^{Skp2} complex is active in the S and G_2 phases.

Two direct substrates of the APC^{Cdh1} and SCF^{Skp2} complexes, Geminin and Cdt1, are involved in "licensing" of replication origins (Nishitani et al., 2000). This carefully regulated process ensures that replication occurs only once in a cell cycle. In higher eukaryotes, proteolysis and Geminin-mediated inhibition of the licensing factor Cdt1 are essential for preventing re-replication. Due to cell cycle-dependent proteolysis, protein levels of Geminin and Cdt1 oscillate inversely. Western blot analysis of
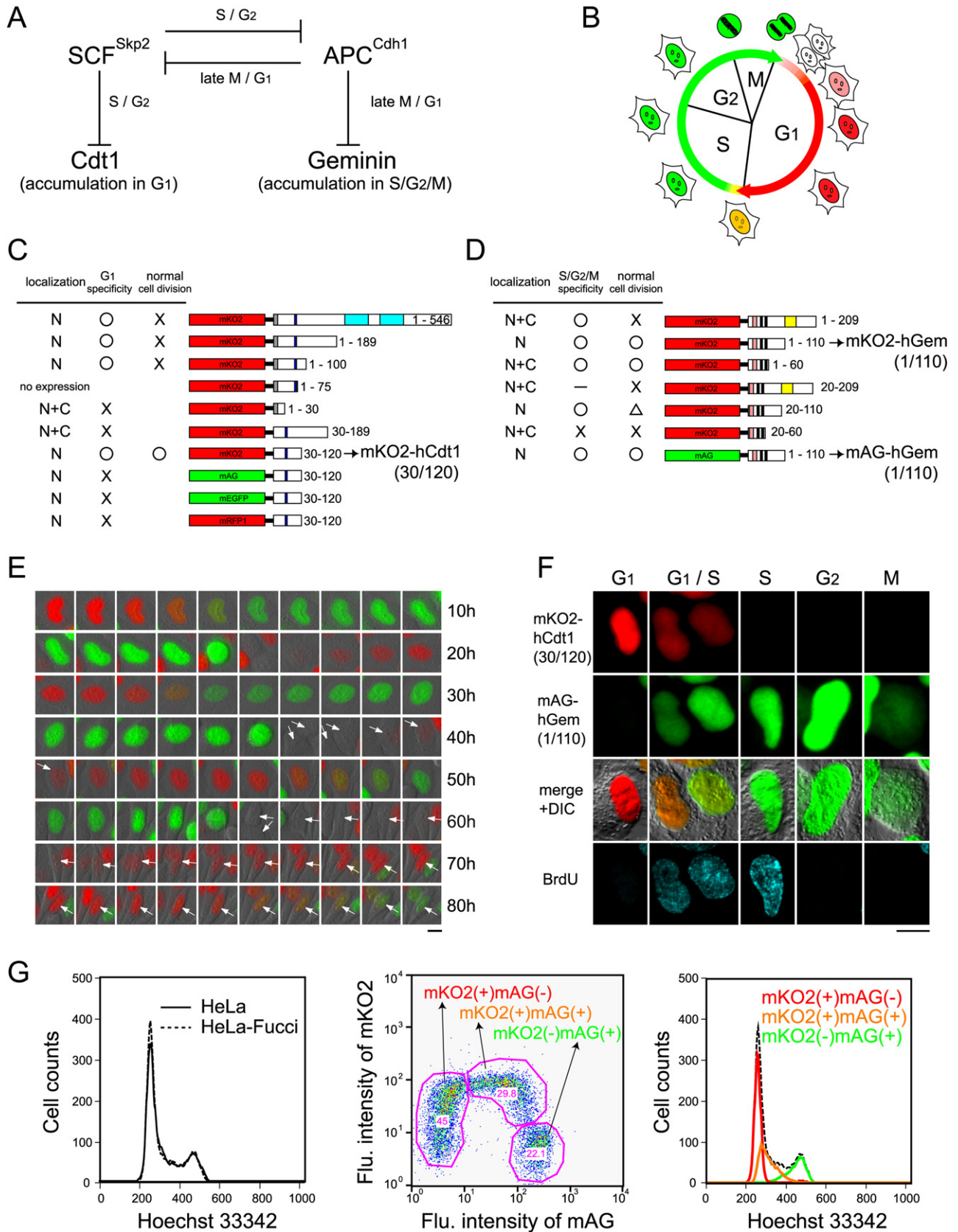
synchronized cultured cells has shown that Cdt1 levels are highest during G_1, while Geminin levels are highest during the S, G_2, and M phases (Nishitani et al., 2004). In this study, we harnessed the regulation of cell cycle-dependent ubiquitination in order to develop two genetically encoded indicators for cell-cycle progression.

RESULTS AND DISCUSSION

Construction of Cell-Cycle Probes

We fused red- and green-emitting fluorescent proteins to E3 ligase substrates, Cdt1 and Geminin, to develop dual-color fluorescent probes that indicate whether individual live cells are in G_1 phase or S/G_2/M phases (Figure 1B). First, a fast-folding variant of mKO (monomeric version of Kusabira Orange) (Karasawa et al., 2004) was generated (H.O.S. Karasawa and A.M., unpublished data) and named mKO2. mKO2 was fused to full-length human Cdt1 (hCdt1) (Figure 1C, [1–546]). When the chimeric protein was expressed in HeLa cells under the control of the ubiquitous CMV promoter, red fluorescence was observed in the nuclei of a fraction of cells. Cells were then time-lapse imaged using computer-assisted fluorescence microscopy (Olympus, LCV100). Cell morphology was monitored by differential interference contrast (DIC) to follow cell division. During the first 48 hr after transfection, we observed a sudden disappearance of red fluorescence, suggesting that mKO2-hCdt1 protein was being degraded by the SCF^{Skp2} complex at the onset of S phase. However, after 48 more hours, we noticed that the transfected cells failed to proceed to mitosis, whereas nontransfected cells divided normally. This is consistent with the fact that overexpression of hCdt1 causes re-replication of DNA (Vaziri et al., 2003; Blow and Dutta, 2005). In addition, we were unable to obtain any healthy stable transformants expressing the chimeric protein.

To overcome the cell-cycle arrest, numerous hCdt1 deletion mutants were constructed and fused to mKO2 (Figure 1C), then evaluated for cell cycle-dependent red fluorescence in the nucleus by time-lapse imaging. As expected, the Cy motif (amino acids 68 – 70), which binds to the SCF^{Skp2} E3 ligase (Nishitani et al., 2006), was required for proper function. Although the N-terminus of hCdt1 (amino acids 1–10) binds to a different E3 ligase (Cul4) (Senga et al., 2006; Nishitani et al., 2006), removal of this region appeared to be critical for the establishment of stable transformants with normal cell division. Since Cdt1 degradation by the SCF^{Skp2} complex has been shown to be independent of its binding to Geminin (Lee et al., 2004; Nishitani et al., 2004; Sugimoto et al., 2004), we also removed the Geminin-binding region. The resulting truncated hCdt1 protein (amino acids 30–120) is sufficient for marking cells in G_1 phase [mKO2-hCdt1(30/120), Figure 1C]. Interestingly, mKO2 in mKO2-hCdt1(30/120) could not be replaced with mAG (the monomeric version of Azami Green) (Karasawa et al., 2003), mEGFP, or mRFP1; the use of these latter fluorescent proteins resulted in constant fluorescence signal throughout the cell cycle (Figure 1C).

Like Cdt1, the cyclin-dependent kinase (Cdk) inhibitor p27 is ubiquitinated by the SCF^{Skp2} complex. Since a p27-luciferase (p27Luc) fusion protein can be used to monitor Cdk2 inhibitor pharmacodynamics in vivo (Zhang et al., 2004), we attempted to fuse fluorescent proteins to p27 or the p27 domains recognized by ubiquitin ligase, but none of the fusions produced bright, cell cycle-dependent fluorescence comparable to that observed with mKO2-hCdt1(30/120) (data not shown).

Next, mKO2 was fused to truncated versions of human Geminin (hGem) (Figure 1D) and tested as described for mKO2-hCdt1. A chimeric protein composed of mKO2 and the 110 amino acid N-terminus of hGem [mKO2-hGem(1/110)] showed the best performance among the constructs tested. It should be noted that mKO2-hGem(1/110) also lacks the Cdt1 binding region (Lee et al., 2004). Unlike hCdt1(30/120), hGem(1/110) could be fused to several other fluorescent proteins. mAG was substituted to generate a green version, mAG-hGem(1/110) (Figure 1D).

Cell Cycle Analysis of Cultured Cells Stably Expressing the Cell-Cycle Probes

We next used lentiviral vectors for coexpression of the two constructs in HeLa cells. Since this gene-transfer technique is highly efficient, cotransduction allowed us to obtain stable transformants expressing equivalent levels of mKO2-hCdt1(30/120) and mAG-hGem(1/110). In each transformant, red fluorescence alternated with green fluorescence in the nucleus (Movie S1 available online). A typical time series is shown in Figure 1E. The cell-cycle period was variable, presumably due to differences in cell density and serum concentration. Since the green fluorescence disappeared rapidly in late M phase and the red fluorescence became detectable in early G_1 phase, a small gap in fluorescence

---

Figure 1. Development and Characterization of a Fluorescent Indicator for Cell-Cycle Progression

(A) Cell-cycle regulation by SCF^{Skp2} and APC^{Cdh1} maintains bistability between G_1 and S/G_2/M phases.

(B) A fluorescent probe that labels individual G_1 phase nuclei in red and S/G_2/M phase nuclei green.

(C) Various constructs with concatenated mKO2 and deletion mutants of human Cdt1 for labeling nuclei in G1 phase. Grey box, QXRVTDF motif (amino acids 1–10); blue box, Cy motif (amino acids 68–70); cyan box, Geminin binding domain (data from mouse Cdt1). Symbols and abbreviations are as follows: ○, pass; ×, failure; N, nucleus; C, cytosol.

(D) Various constructs with concatenated mAG and deletion mutants of human Geminin for labeling nuclei in S, G2, and M phases. Pink box, D (destruction) box; black box, NLS; yellow box, coiled coil domain (Cdt1 binding domain). Symbols and abbreviations are as follows: ○, pass; ×, failure; Δ, marginal; —, not determined; N, nucleus; C, cytosol.

(E) Cell cycle-dependent changes in fluorescence of mKO2-hCdt1(30/120) and mAG-hGem(1/110) in HeLa cells. Arrows indicate cells that were tracked. The scale bar represents 10 μm.

(F) Typical fluorescence images of HeLa cells expressing mKO2-hCdt1(30/120) and mAG-hGem(1/110) and immunofluorescence for incorporated BrdU at G_1, G_1/S, S, G_2, and M phases. The scale bar represents 10 μm.

(G) HeLa cells showing red [mKO2(+)mAG(-)], yellow [mKO2(+)mAG(+)], and green [mKO2(-)mAG(+)] fluorescence were collected, and their DNA contents were stained with Hoechst33342 and measured using a fluorescence-activated cell sorter.

was observed in newborn daughter cells. By contrast, during red-to-green conversion, red and green fluorescence always overlapped to yield a yellow nucleus. To examine whether the timing of the color conversion correlates with the onset of S phase, transformants were pulse-labeled with BrdU for five minutes and immediately immunostained for BrdU. Typical confocal images of cells at the G1/S transition and in the G_1, S, G_2, and M phases are shown in Figure 1F (see Figures S1A–S1D for a wide-field image). Since all of the cells with yellow nuclei showed BrdU incorporation, the emergence of the green fluorescence is indicative of the initiation of the S phase. Similar results were obtained from a separate experiment in which we immunostained for PCNA (Bravo and Macdonald-Bravo, 1987) (Figure S1E). Cells with nuclei emitting pure green fluorescence were also observed. These cells were either in the S or G_2 phase, and were distinguishable by nuclear BrdU or PCNA immunostaining. These results are consistent with the fact that Cdt1 accumulates in G_1, while Geminin accumulates in $S/G_2/M$ phases.

We named this *f*luorescent, *u*biquitination-based *c*ell *c*ycle *in*-dicator, "Fucci." Analysis of DNA content by flow cytometry revealed the same distribution between Fucci-expressing and parental HeLa cells (Figure 1G, left). Cells expressing Fucci were divided into red-, yellow-, and green-emitting populations [mKO2(+)mAG(-), mKO2(+)mAG(+), mKO2(-)mAG(+), respectively] (Figure 1G, middle), and their DNA contents were analyzed following Hoechst33342 staining. Green and yellow cells had fully- and partially-replicated complements of DNA, respectively (Figure 1G, right). Thus, differential profiling of cells at G_1 and $S/G_2/M$ phases can be achieved by sorting a population of cells into red, yellow, or green and examining various cellular functions, such as gene expression and antigen surface expression. Stable transformants constitutively expressing Fucci were obtained using other cell lines, including normal murine mammary gland (NMuMG) cells, PC12 cells, and COS7 cells.

Monitoring Structural and Behavioral Changes and Cell-Cycle Dynamics of Cultured Cells

The epithelial-mesenchymal transition (EMT) is a fundamental morphogenetic process by which mesenchymal cells are formed from epithelia during embryonic development, wound repair, and tumor progression in multicellular organisms (Thiery and Sleeman, 2006). In vitro EMT is characterized by dissolution of cell-cell junctions, cytoskeletal rearrangements, and increased motility of cultured cells. It is possible that specific stages of the cell cycle are involved in the process. Indeed, it was recently reported that transforming growth factor β (TGFβ) efficiently induced EMT in AML-12 hepatocytes synchronized at the G1/S phase, but not in cells synchronized at the G2/M phase (Yang et al., 2006). Moreover, NMuMG cells undergo EMT in response to TGFβ (Piek et al., 1999; Tojo et al., 2005).

To examine cell-cycle progression during EMT, we examined Fucci-expressing, stably transformed NMuMG cells. After cells were plated on a glass coverslip, they proliferated as clusters maintaining cell-cell adhesion with their neighbors (Figure 2A, 1 hr). The high proliferation rate of these cells was evidenced by the large fraction of cells with green nuclei (Figure 2A, 25–49 hr). However, at confluence, the green nuclei were replaced with red nuclei (Figure 2A, 73 hr), indicating that cells remained

in G_1 phase (Movie S2, left). When we introduced a wound in the confluent monolayer (Figure 2C, 1 hr), cells at the edge of the wound turned green (Figure 2C, 13 hr, arrows), indicating that closure of the wound required proliferation of NMuMG cells. Notably, the green nuclei appeared 9-13 hr after wound induction. Such a time delay of more than 8 hr was reproducibly observed in other similar wound healing experiments and is reminiscent of the 8 hr required for NIH 3T3 cells to re-enter the cycle from a state of quiescence (G_0) after the onset of proliferation stimuli (Zetterberg and Larsson, 1985). It is thus possible that the confluent NMuMG cells (Figure 2A, 85 hr) remained in G_0 phase.

Next, we performed the same experiments in the presence of 1 ng/ml of TGFβ. Within one day following TGFβ treatment, the number of cells with green nuclei increased (Figure 2B, 1–49 hr), indicating that this ligand induced a G1/S transition. Subsequently, cells began to adopt a spindle-shaped, fibroblast-like morphology and high motility (Figure 2B, 49 hr). After two days of TGFβ treatment, the number of cells with green nuclei diminished, reflecting the G_1 arrest effect of TGFβ (Figure 2B, 49–85 hr) (Movie S2, right). Thus, TGFβ-treated cells spread without proliferation, in contrast with the untreated NMuMG cells, which were densely packed in a confluent monolayer. In addition, the introduction of a wound did not result in proliferation, but rather a further expansion of cells (Figure 2D).

Cell-Cycle Progression of Tumor Cells in Live Mice

Whole-body and intravital cellular imaging of mice injected with cultured tumor cells genetically labeled with fluorescent proteins has proven to be a powerful technique for investigating tumor development (Hoffman, 2005; Yamauchi et al., 2006). We tested whether or not Fucci could be used to monitor tumor development by subcutaneously injecting Fucci-expressing NMuMG cells into the mammary fat pad of nude mice (Figure 3A). One day after inoculation, both green and red cells were observed (Figure 3B). After 16 days, however, only red cells were seen (Figure 3C), indicating that NMuMG cells are nontumorigenic. Next, Fucci-expressing HeLa cells were injected in a similar fashion into nude mice (Figure 3D). The injected cells gradually grew and emitted both green and red fluorescence for a month, suggesting tumor progression (Figures 3E and 3F). The expanded mass was observed through the skin under a microscope (Olympus, IV100, 10×, UplanFL N N.A. = 0.30) 27 days after injection (Figure 3G). Well-developed tumor vessels were visualized by loading AngioSense750, which emits far-red fluorescence. Although triple-color live imaging identified HeLa cells in G_1 and S/G_2 phases, their positions relative to the vessels were not clear due to the low spatial resolution. The tumor was fixed, sectioned, and stained with an antibody against CD31. Both the red and green fluorescence of Fucci remained after conventional immunostaining procedures, including fixation in 4% PFA. The cell-cycle phase pattern of HeLa cells around blood vessels was clearly visualized (Figure 3H). The pattern appeared to depend on several factors, including the maturity of vessels and the degree of necrosis in the surrounding tissues. A statistical analysis is underway to investigate these relationships.

Next, cell-cycle progression of tumor cells was examined during the initial steps of the classic metastatic cascade, such as
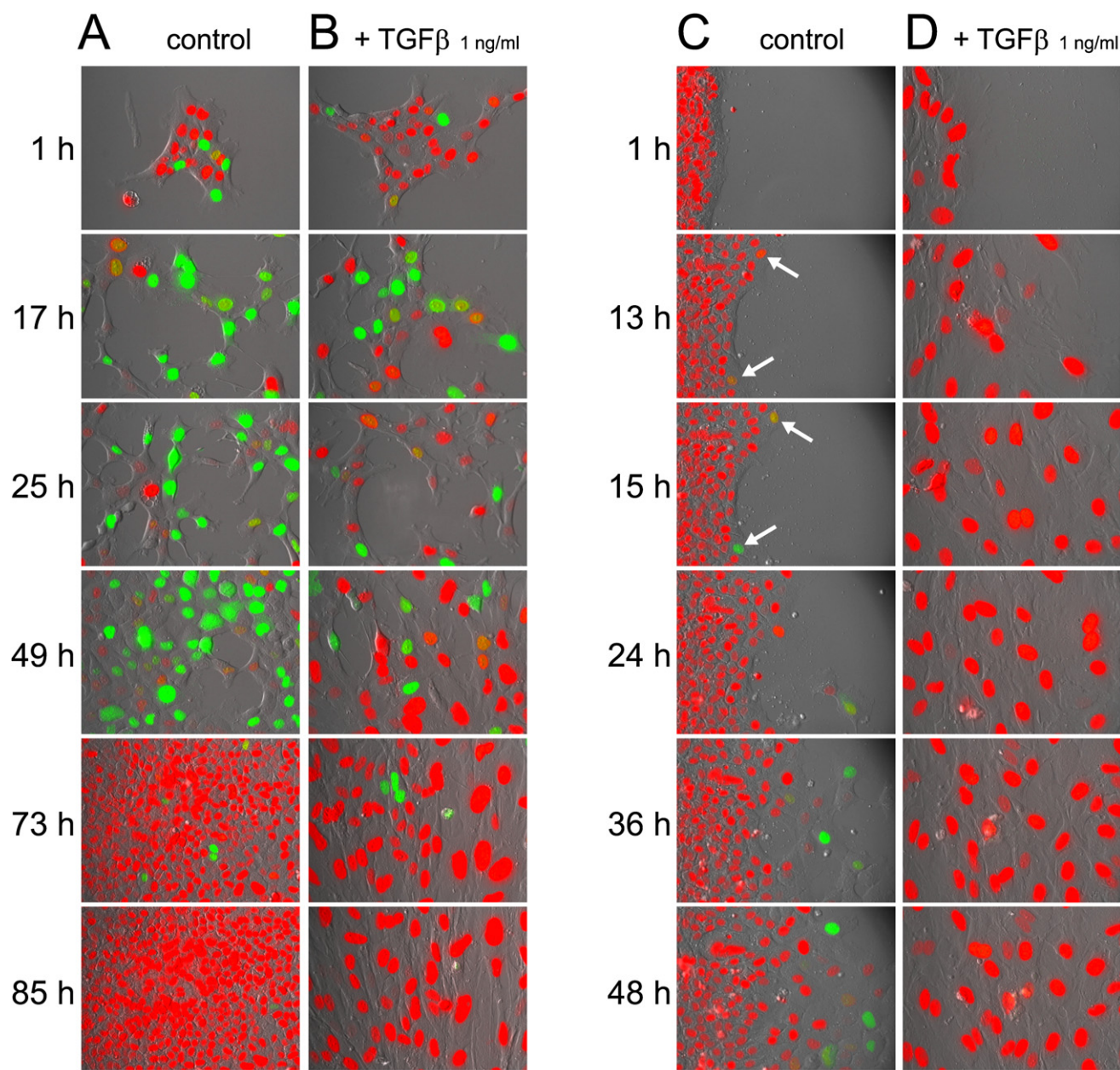
Figure 2. Cell-Cycle Regulation of Cultured NMuMG Cells

(A and B) Fluorescence images of Fucci-expressing NMuMG cells in the absence (A) and presence (B) of TGFβ (1 ng/ml) while reaching a confluent monolayer state.

(C and D) Fluorescence images of Fucci-expressing NMuMG cells in the absence (C) and presence (D) of TGFβ (1 ng/ml) after the monolayer was scratched. Two nuclei entering S phase at 13 hr are indicated by arrows in (C). The scale bar represents 50 μm.

adhesion to endothelial cells and extravasation. Fucci-expressing HeLa cells in a gel were injected into a skin vein (Figure S2), and intravital cellular imaging was performed. Interestingly, at early stages, nearly all of the cells attached to the inner wall of the veins were in G_1 phase (Figures 3I and 3J). We captured an image of a cell in the process of extravasation (Figures 3K, 3L, and 3M). Within a cluster of HeLa cells across a vein wall, an elongated cell with a yellow, fragmented nucleus was observed to pass through the wall. Four days postinjection, HeLa cells were found to invade and proliferate over the veins (Figures 3N and 3O), suggesting multiple occurrences of extravasation.

Previous work showed that cultured cells with differentially labeled cytoplasm and nuclei that were injected into mice could be used to image nuclear-cytoplasmic dynamics in order to monitor
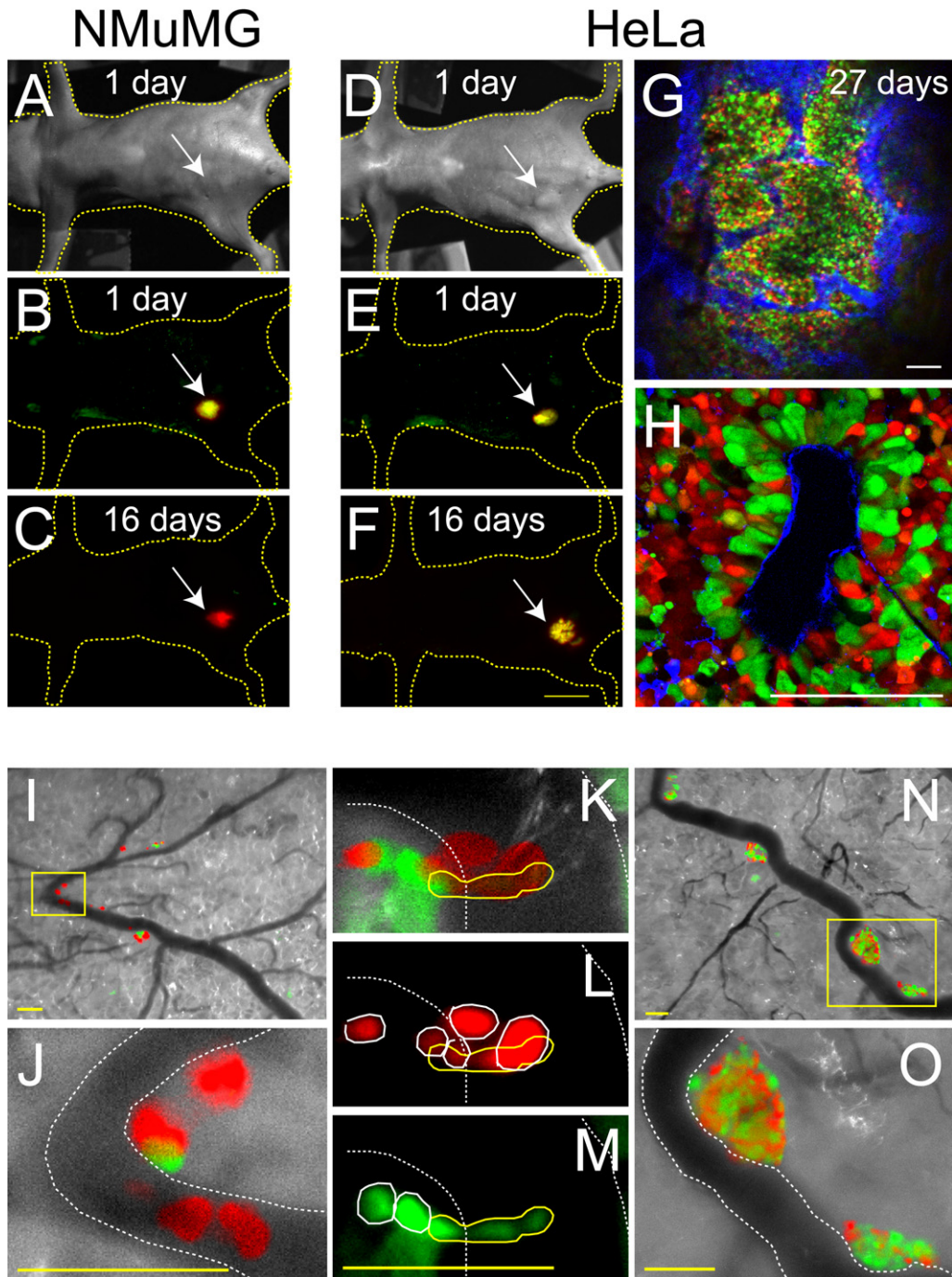
Figure 3. Cell-Cycle Progression of Cultured Cells Injected into Live Mice

(A–H) Observation of Fucci-expressing cultured cells subcutaneously inoculated into the mammary fat pad of nude mice. (A–C) Fucci-expressing NMuMG cells. (D–H) Fucci-expressing HeLa cells. (A–F) Whole-body images were acquired using the Olympus OV100 Imaging System with a 0.14× objective lens and F-View II camera (Soft Imaging System). The scale bar represents 1 cm. (A, B, D, and E) 1 day postinoculation. (C and F) 16 days postinoculation. (A and D) bright-field images. (B, C, E, and F) Red and green fluorescence images were merged. The yellow mass (B, E, and F) consisted of both red and green nuclei, while the red mass (C) consisted predominantly of red nuclei. (G) A triple-color intravital cellular image of the expanded mass of HeLa cells 27 days post inoculation. Tumor vessels were visualized (blue) after loading the mouse with AngioSense750. Image acquisition was performed using an IV100 intravital laser scanning microscope (Olympus). The scale bar represents 100 μm. (H) A triple-color image of a section of the fixed mass. Vessels were stained for CD31 and displayed in blue. Image acquisition was performed using an FV1000 confocal microscope system. The scale bar represents 100 μm.

(I–O) Observation of Fucci-expressing HeLa cells after injection into an epigastrica cranialis vein. Fluorescence images were acquired using the Olympus OV100; red and green images were merged and superimposed on DIC images. Vessels are delineated with white dotted lines. The scale bar represents 100 μm. (I and J)

cancer cell trafficking, deformation, extravasation, mitosis, and cell death in live mice (Yang et al., 2003). In combination with these cytoplasmic labeling techniques, fluorescence imaging of stably transformed Fucci-expressing cells injected into live animals will provide reliable pharmacodynamic readouts for the growth and metastatic behavior of tumors.

Cell Cycle Analysis of Developing Neural Tissue in Fucci Transgenic Mice

One major advantage of our genetically encoded probe is that it need not depend on transcriptional regulation; its transcription can be driven using constitutive promoters. Thus, we can easily generate transgenic organisms for cell cycle analysis. Using the CAG promoter (Niwa et al., 1991), we have made transgenic mouse lines that ubiquitously express mKO2-hCdt1(30/120). From 16 mouse lines emitting red fluorescence, #596 was selected for further characterization. We also made eight green fluorescent mAG-hGem(1/110) mouse lines from which #504 was chosen for further characterization. These mouse lines provide us with an unprecedented model system with which to study the coordination of the cell cycle and development. #504 is particularly useful because it provides in vivo information about proliferation patterns. During early development of the mammalian cerebral cortex, neural progenitors in the ventricular zone (VZ) undergo expansion. To determine whether mAG-hGem(1/110) green fluorescence is produced by neural progenitors, we performed immunohistochemistry on telencephalic sections of an embryonic day (E)14 #504 transgenic embryo. Since the telencephalic cells with green nuclei were immunopositive for Nestin but not MAP2 (Figure S3), these cells were likely to be neural progenitors.

Next, we crossbred #596 and #504 transgenic mice to generate a mouse line producing Fucci, in which every somatic cell nucleus exhibited either red or green fluorescence. We fixed an E13 Fucci transgenic embryo and prepared coronal sections of the brain. Red and green fluorescence was examined in every section using confocal laser scanning microscopy. Fluorescence images of three representative sections are shown in Figures 4A, 4E, and 4I. The red and green signals appear to be well balanced at the embryonic stage, but the overall ratio of green-to-red signal decreases as the mice grow (data not shown).

In the developing cerebral cortex (Figures 4B, 4F, 4G, and 4J), nuclei emitting red mKO2-hCdt1(30/120) fluorescence were identified in two main cell populations: mitotic neural progenitors in the VZ and postmitotic neurons destined to populate different layers in the cortical plate (CP). The postmitotic neurons exhibited much brighter red fluorescence, probably due to accumulation of mKO2-hCdt1(30/120) after cell-cycle exit. The bright red nuclei of blood vessels were also visible in the VZ of the dorsal telencephalon (Figures 4B and 4F). It is interesting to note that in the diencephalon there was a stripe of cells in G_1 phase, which corresponded to the zona limitans intrathalamica (zli). The dorsal thalamus contained more green nuclei than the ventral thalamus (Figures 4I and 4J), which suggests that cells in the ventral region

undergo cell-cycle exit for differentiation prior to those in the dorsal region.

The differential intensity of red fluorescence between mitotic and postmitotic cells was observed also in the developing neuroepithelia of the olfactory and vomeronasal systems (Figures 4C and 4D, respectively) and the retina (Figure 4H). The random distribution of high- and low-intensity fluorescent nuclei may suggest that the architecture of the olfactory and vomeronasal epithelia is not yet established at E13. In contrast, bright red nuclei were observed in the central apical region of the developing retina (Figure 4H), whose developing retinal ganglion cells undergo centrifugal differentiation (Neumann and Nuesslein-Volhard, 2000). The epithelial cells of the lens had also exited the cell cycle by this stage. Other extra-neural tissues with bright red fluorescence include the trigeminal ganglion (Figure 4K) and pituitary gland (Figure 4L).

Coronal sections of mouse embryos (E13) were also examined immunohistochemically. Proliferation was visualized by nuclear immunostaining for BrdU (Figure S4) or PCNA (Figure S5). PCNA images were merged with fluorescence images of mKO2-hCdt1(30/120) to indicate neuronal differentiation. The balance between proliferation and differentiation in the telencephalon, diencephalon, olfactory vesicle, and retina (Figures S4 and S5) was very similar to that observed through the green and red signals of Fucci (Figure 4).

Geminin and Cdt1 were previously shown to be abundantly expressed by neural progenitors during early mouse neurogenesis, but transcriptionally downregulated at late developmental stages (Spella et al., 2007). It should be again noticed that Fucci signal is not affected by transcriptional regulation in our transgenic mice.

In the developing cerebral cortex, some neural progenitors exit the cell cycle and migrate beyond the VZ, where they differentiate into neurons or, at later stages, into glial cells. Neural progenitors also undergo a typical migration pattern within the VZ; their nuclei undergo characteristic movements, known as interkinetic nuclear movements (Sauer, 1935). M-phase nuclei are located on the ventricular surface, while S-phase nuclei are farther from the ventricle. In order to observe the spatial and temporal regulation of proliferation, differentiation, and migration of neural progenitors, we performed time-lapse imaging experiments using slices of dorsal telencephalon prepared from an E13 Fucci transgenic embryo (Figure 5A). Time-lapse imaging experiments using acute cortical slices are usually acquired at >3 hr intervals. With such long intervals, neither nuclear movements nor cell-cycle progression can be adequately followed. However, the bright Fucci fluorescence enables 3D time-lapse imaging with 10 min intervals in the xyz-t mode using the FV1000 multiposition stage system. At each time point, 20 confocal images along the z-axis (2 μm step) were acquired. In addition, exposure of slices to 40% oxygen, instead of the usual 20%, has significantly improved cell proliferation, differentiation, and migration during imaging experiments (Miyata et al., 2002, 2004). As mentioned earlier, the red nuclei of mitotic neural progenitors were much dimmer than

---

At an early stage, most of the cells remaining in vessels were in G_1 phase. The box region in (I) is expanded and shown in (J). Two HeLa cells with red nuclei attached to the inner surface of the vein. (K–M) An image of the process of extravasation. Red (L) and green (M) fluorescent images showing the presence of a cell with an elongated, yellow nucleus. (N and O) 4 days postinjection. The box region in (N) is expanded and shown in (O).
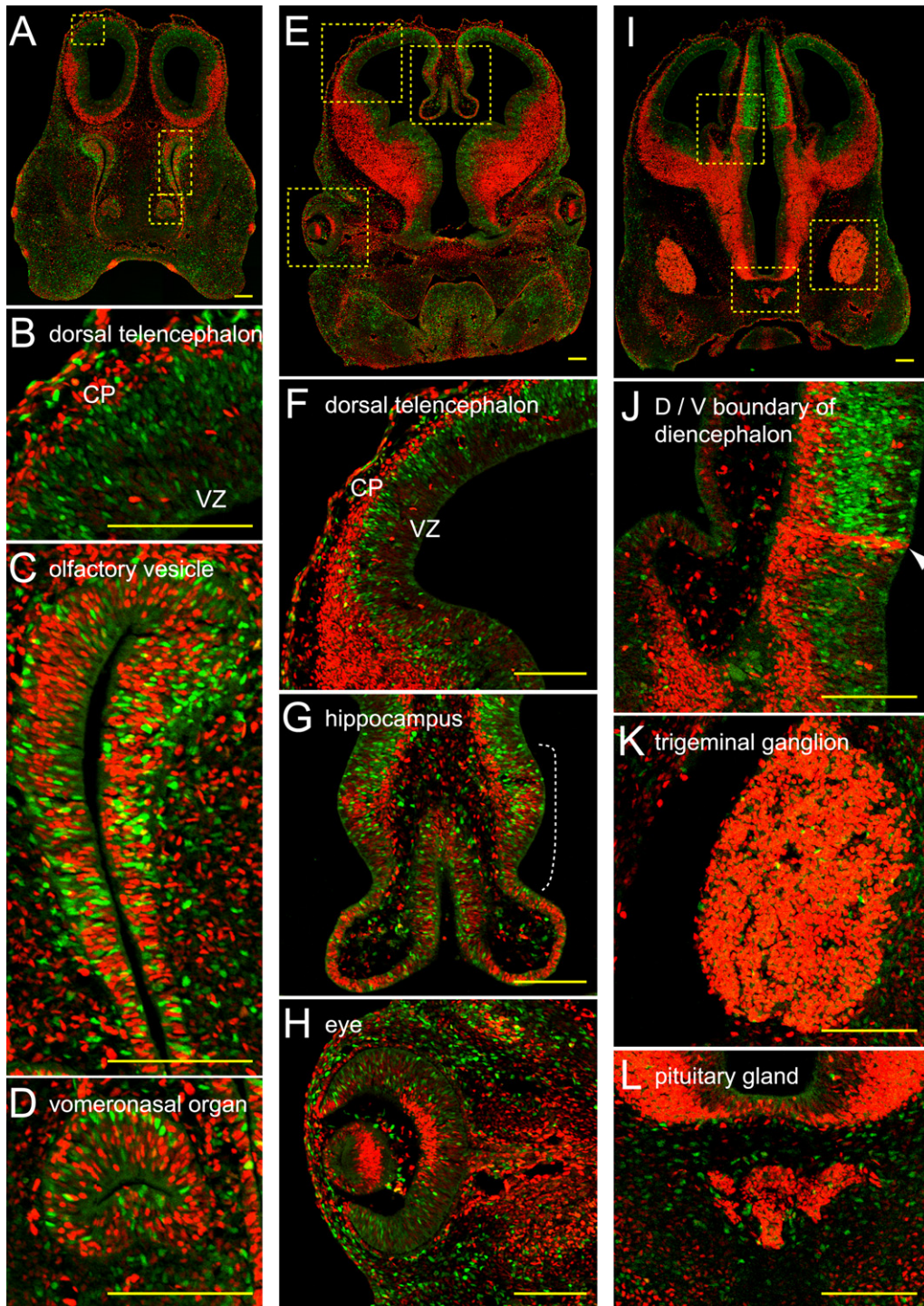
Figure 4. A Survey of the Cell Cycle in the Developing Mouse Head

Coronal sections of an E13 Fucci transgenic embryo. Red and green fluorescence signals are merged. The scale bar represents 100 μm.

(A–D) The section containing the brain, olfactory system, and vomeronasal system. The box regions in (A) are expanded in (B), dorsal telencephalon, (C), olfactory vesicle, and (D), vomeronasal organ.

(E–H) Section containing the brain, hippocampus, and eye. The boxed regions in (E) are expanded in (F), dorsal telencephalon, (G), hippocampus, and (H), eye.

(I–L) Section containing the brain, trigeminal ganglion, and pituitary gland. The box regions in (I) are expanded in (J), the dorsal/ventral boundary of diencephalon, (K), trigeminal ganglion, and (L), pituitary gland.

A

B

CP
IZ
VZ

IZ

VZ

C

CP

IZ

M

VZ

M

M
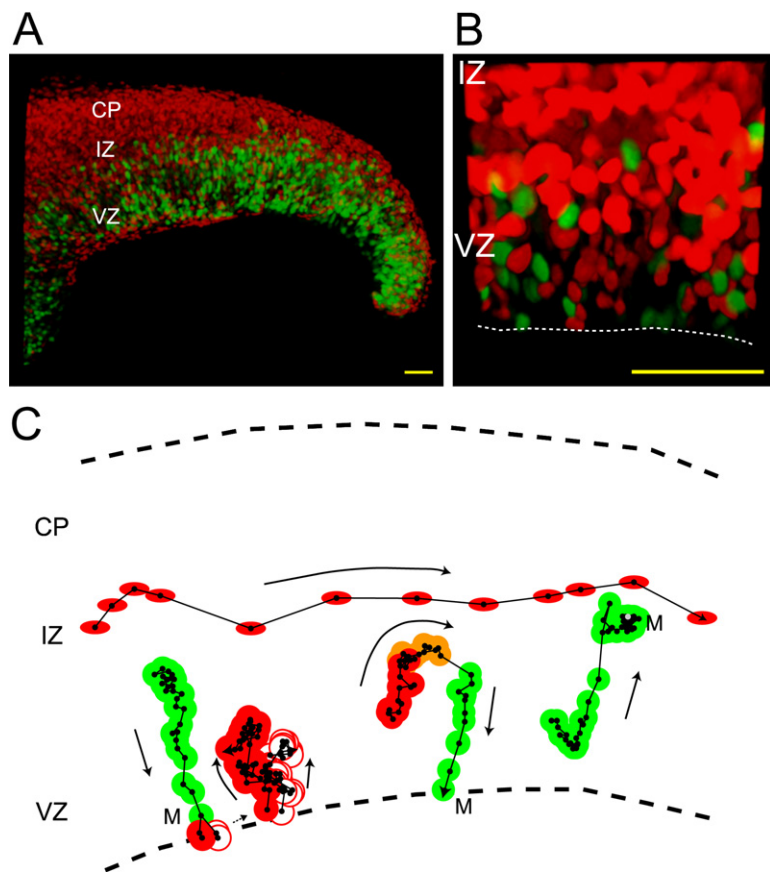
Figure 5. Cell Cycle-Related Migration of Nuclei in the Dorsal Telencephalon of an E13 Fucci Transgenic Mouse Embryo

Abbreviations are as follows: CP, cortical plate; IZ, intermediate zone; VZ, ventricular zone. The scale bar represents 100 μm.
(A) A cultured slice for 3D time-lapse imaging.
(B) An expanded image of the IZ and VZ with red fluorescence detection sensitivity increased.
(C) A schematic diagram showing migration of neural progenitors (bottom) and an interneuron (top) in the cultured slice. Abbreviation is as follows: M, M phase. Entry into prometaphase can be detected by the spread of green fluorescence throughout the cell due to breakdown of the nuclear envelope.

those of postmitotic ones. To visualize migration of the nuclei in the cell cycle within the VZ, we increased the photomultiplier tube (PMT) sensitivity for red fluorescence. While nuclei in the CP showed saturated red fluorescence, nuclei in the VZ exhibited equivalent levels of either green or red fluorescence (Figure 5B). Under these conditions, the change in color between green and red during cell-cycle progression and the migration of cells could be clearly followed. First, we followed the trajectories of VZ neural progenitor nuclei corresponding to interkinetic nuclear movements. The trajectory of a migrating cell along with its cell-cycle progression from S/G_2 to G_1 and cell division at the ventricular surface is illustrated in Figure 5C (left). A green nucleus descended in the VZ and completed mitosis upon reaching the ventricular surface. Then, the two daughter nuclei turned red and started migrating away from the surface. Another nucleus that progressed from G_1 to M (Figure 5C, middle) underwent the G_1/S transition while making a hairpin turn near the intermediate zone (IZ). In addition, we observed nuclear migration, which might be involved in nonsurface mitoses (Haubensak et al., 2004; Noctor et al., 2004); a green nucleus was observed to wander about in the IZ until it entered M phase (Figure 5C, right). Finally, we observed bright red nuclei traveling quickly in the IZ from the ventral to dorsal part of the telencephalon (Figure 5C, top). These nuclei are likely to belong to cortical GABA (γ-amino-butyric acid) neurons, which are born in the subpallial telencephalon and migrate tangentially to reach their final destination (Marín and Rubenstein, 2001).

Fucci Is Compatible with Established Imaging Protocols

The nuclear localization of Fucci is advantageous in the following respects: additional far-red fluorescent proteins that are spectrally distinct from both mAG and mKO2, such as mCherry (Shaner et al., 2004) and mKeima (Kogure et al., 2006), can be expressed in the cytoplasm by tagging them with Nuclear Export Signal (NES), in order to identify cell types and observe cell morphology. The third color fluorescence signal can also be provided by chemical dyes. In the experiment shown in Figure 5, we placed fine DiD crystals on the pial surface of the brain slice to sparsely label pia-connected progenitors. The bipolar morphology of a progenitor with a green nucleus whose movement was tracked (Figure 5C, left) could be identified. The DiD image at a particular time point (indicated by an arrow in Figure 5C) is shown in Figure S6. The excitation and emission spectra of Fucci and possible complementary dyes are presented in Figure S7.

Many genetically encoded indicators that utilize Green Fluorescent Protein (GFP)-based Fluorescence Resonance Energy Transfer (FRET), including cameleon (Miyawaki et al., 1997) and Raichu-Ras (Mochizuki et al., 2001), are distributed in the cytoplasm. Thus, cell-cycle phase can be monitored in parallel with signaling events taking place in the cytoplasm. For instance, we transfected Raichu-Ras (Raichu 124X) into Fucci-expressing COS7 cells, and observed that K-ras was more active in G_1 phase than in S/G_2 phase in response to epidermal growth factor signaling (Figure S8). Thus, the cell-cycle dependency of numerous cellular events can be elucidated without using cell-cycle synchronization techniques. Multicolor imaging in combination with these fluorescent probes and proteins will further expand the applications of the Fucci technology.

Future Perspectives of the Fucci Technology

The Fucci technology allows dual-color imaging, which can distinguish between live cells in the G_1 and the $S/G_2/M$ phases. This technology allows for in vivo analysis of spatial and temporal patterns of cell-cycle dynamics, owing to the brightness of the fluorescence and the high contrast between the two colors (red and green). Although Fucci is composed of mKO2-hCdt1(30/120) and mAG-hGem(1/110), single transfection of either would

suffice in conferring the cell-cycle indicator function; for instance, the transgenic mouse line #504 just produces mAG-hGem(1/110) but nevertheless provides in vivo information about proliferation patterns. However, coexpression of both constructs is still considerably more useful because it highlights the G$_1$/S transition with a yellow signal, and because it permits us to continuously track migrating cells or nuclei in the cell cycle. In this regard, reliable gene-transfer techniques which control the stoichiometry of two constructs will be required.

Future challenges involve further developing the Fucci derivatives (1) with different colors so that coexpressed GFP or RFP can be spectrally distinguished, (2) that highlight cell-cycle transitions other than G$_1$/S, and (3) that function in nonmammalian cell types. Such research will benefit from exploration of the molecular mechanisms underlying both cell-cycle progression and ubiquitin-mediated protein degradation. Regarding the last challenge, it should be noted that the primary structures of Cdt1 and Geminin vary among species. By tagging certain domains of the lower eukaryotic homologs of these two proteins to mKO2 or mAG, we have developed a version of Fucci that functions in fish and insect cells (data not shown). We have also generated transgenic zebrafish and *Drosophila* lines expressing the non-mammalian Fucci in an effort to investigate the spatial and temporal regulation of cell-cycle progression during major morphogenetic events such as gastrulation and metamorphosis, and during basic morphogenetic processes such as invagination, involution, and branching.

EXPERIMENTAL PROCEDURES

Gene Construction

mKO2 was developed by introducing eight mutations (K49E, P70V, F176M, K185E, K188E, S192D, S196G, and L210Q) into mKO (Karasawa et al., 2004). mKO2 absorbs light maximally at 551 nm (molar extinction coefficient, 63,800 M^{-1}cm^{-1}) and emits fluorescence at 565 nm (fluorescence quantum yield, 0.57). mKO2 and mAG cDNAs (Medical Biological Laboratory, Amalgaam) were amplified using primers containing 5′-EcoRI and 3′-*Eco*RV sites, and digested products were cloned in-frame into the EcoRI/*Eco*RV sites of pcDNA3 (Invitrogen) vector to generate pcDNA3/mKO2 and pcDNA3/mAG, respectively. The entire or numerous partial cDNA species of human Cdt1 (GenBank: NM_030928) or human Geminin (GenBank: NM_015895) were amplified using primers containing 5′-*Xho*I and 3′-*Xba*I sites, and digested products were cloned in-frame into the *Xho*I/*Xba*I sites of pcDNA3/mKO2 or pcDNA3/mAG.

Cell Culture

HeLa cells and COS7 cells were grown in DMEM supplemented with 10% fetal bovine serum and penicillin/streptomycin. Mouse NMuMG breast epithelial cells were grown in DMEM (high glucose) medium supplemented with 10% fetal bovine serum, penicillin/streptomycin, and 10 μg/ml Insulin (Sigma). EGF and TGFβ1 were purchased from R&D.

Imaging of Cultured Cells

Cells were grown on a 35 mm glass-bottom dish in phenol red-free Dulbecco's modified Eagle's medium containing 10% fetal bovine serum (FBS). Cells were transiently or stably transfected with cDNA using Lipofectin (Invitrogen) and subjected to long-term, time-lapse imaging using a computer-assisted fluorescence microscope (Olympus, LCV100) equipped with an objective lens (Olympus, UAPO 40×/340 N.A. = 0.90), a halogen lamp, a red LED (620 nm), a CCD camera (Olympus, DP30), differential interference contrast (DIC) optical components, and interference filters. For fluorescence imaging, the halogen lamp was used with two filter cubes, one with excitation (BP520-540HQ)

and emission (BP555-600HQ) filters for observing mKO2 fluorescence, and the other with excitation (470DF35) and emission (510WB40) filters for observing mAG fluorescence. For DIC imaging, the red LED was used with a filter cube containing an analyzer. Image acquisition and analysis were performed by using MetaMorph 6.13 software (Universal Imaging, Media, PA).

Lentivirus Construction and Production

Replication-defective, self-inactivating lentivirus vectors were used (Miyoshi et al., 1997, 1998). cDNA encoding mKO2-hCdt1(30/120) or mAG-hGem(1/110) was cloned into a CSII-EF-MCS vector. The plasmid was cotransfected with the packaging plasmid (pCAG-HIVgp) and the VSV-G- and Rev-expressing plasmid (pCMV-VSV-G-RSV-Rev) into 293T cells. High-titer viral solutions for mKO2-hCdt1(30/120) and mAG-hGem(1/110) were prepared and used for cotransduction into several cell lines: HeLa, COS7, NMuMG, and PC12 cells.

Immunocytochemical Cell Cycle Analysis

Fucci-expressing HeLa cells grown on a coverslip were treated with BrdU (Sigma) for 5 min at 37°C. After being washed with PBS(−), cells were fixed with 4% PFA for 10 min at 4°C and then with 0.1% Triton X-100/PBS(−) for 5 min at room temperature. The antibodies used were: mouse anti-BrdU mAb (ImmunologicalsDirect), mouse anti-PCNA mAb (DAKO), and goat anti-mouse IgG conjugated with Alexa Fluor 633 (Molecular Probes). Image acquisition was performed using an FV500 (Olympus) confocal microscope system equipped with 488 nm (argon), 543 nm (He/Ne), and 633 nm (He/Ne) laser lines.

Flow Cytometry

Hoechst 33342 solution (56 μl of 1 mg/ml stock) (DOJINDO) was added to a 10 cm dish containing parental or Fucci-expressing HeLa cells. After incubation for 30 min, cells were harvested and analyzed using BD LSR (Becton Dickinson). Both mKO2 and mAG were excited by a 488 nm laser line (argon), and Hoechst 33342 was excited by a 325 nm laser line (HeCd). Fluorescence signals were collected at 530 nm (530/28 BP)(FL1) for mAG, at 575 nm (575/26 BP)(FL2) for mKO2, and at 400 nm (380 LP) (FL5) for Hoechst33342. The data were analyzed using FlowJo software (Tree Star).

Generation of Transgenic Mice

cDNA encoding mKO2-hCdt1(30/120) or mAG-hGem(1/110) was cloned into a pCAGGS vector (Niwa et al., 1991). The transgenic insert, devoid of vector sequences, was gel-purified and microinjected into the pronuclei of zygotes of BDF1 inbred mice. Screening for fluorescent founders was performed by illumination with a blue LED (for mAG) and a green LED (for mKO2). 16 lines expressing mKO2-hCdt1(30/120) and eight lines expressing mAG-hGem(1/110) were obtained. The experimental procedures and housing conditions for animals were approved by the Institute's Animal Experimental Committee, and all animals were cared for and treated humanely in accordance with the Institutional Guidelines for Experiments using Animals.

Whole-Body Imaging of Mice

Subcutaneous and intravenous injection of cultured cells, and whole-body imaging with OV100 (Olympus) were performed as described elsewhere (Hoffman and Yang, 2006). To visualize blood vessels, Angio Sense-IVM750 (VisEn medical) was injected, or endothelial cells were stained using anti-CD31 mAb (Chemicon).

Histological Observation of Tissue Sections

E13 Fucci (#596/#504) embryos were perfused transcardially with fixative (4% PFA), placed in ice-cold fixative for 2 hr, cryoprotected in PBS containing 20% sucrose, and embedded in OCT compound. Coronal head sections (15 μm thick) were imaged using FV1000 equipped with two laser diodes (473 nm and 559 nm). The images were tiled to create wide-field pictures. Brain sections from an E14 #504 embryo were fixed, incubated with mouse anti-MAP2 mAb (Chemicon) or mouse anti-Nestin mAb (PharMingen), followed by goat anti-mouse IgG conjugated with AlexaFluor 546X (Molecular Probes).

Imaging of Cultured Brain Slices

Brain slices were prepared from Fucci-expressing mice (#596/#504) at E13, and cultured in collagen gel as previously described (Miyata et al., 2002). Slices

were exposed to 5% CO_2 and 40% O_2. Time-lapse 3D imaging was performed in the xyz-t mode using the FV1000 multiposition stage system. The recording interval was 10 min. At each time point, 20 confocal images along the z-axis (2 μm step) were acquired. To avoid crossdetection of green and red signals, images were acquired sequentially at 488 nm (Argon) and 543 nm (He/Ne). Green and red images were merged for each confocal image. Proper alignment and correct image registration of FV1000 with the two laser lines and detection channels were verified using double-labeled fluorescent beads (Tetra-Speck Fluorescent Microsphere Standards, 0.5 μm in diameter, Molecular Probes). Data analysis was performed using Volocity software (Improvision) and METAMORPF software (Universal Imaging, Media, PA).

Distribution of Materials

DNA constructs such as mKO2-hCdt1(30/120) and mAG-hGem(1/110), their stable transformant cell lines, and transgenic mouse lines reported in this paper will be distributed with concomitant purchase of cDNA for mKO2 or mAG from MBL International (Amalgaam) (http://www.mblintl.com/mbli/index.asp).

Supplemental Data

Supplemental Data include eight figures and three movies and can be found with this article online at http://www.cell.com/cgi/content/full/132/3/487/DC1/.

REFERENCES

Ang, X.L., and Harper, J.W. (2004). Interwoven ubiquitination oscillators and control of cell cycle transitions. Sci. STKE 242, pe31.

Benmaamar, R., and Pagano, M. (2005). Involvement of the SCF complex in the control of Cdh1 degradation in S phase. Cell Cycle 4, 1230–1232.

Blow, J.J., and Dutta, A. (2005). Preventing re-replication of chromosomal DNA. Nat. Rev. Mol. Cell Biol. 6, 476–486.

Bravo, R., and Macdonald-Bravo, H. (1987). Existence of two populations of cyclin/proliferating cell nuclear antigen during the cell cycle: Association with DNA replication sites. J. Cell Biol. 105, 1549–1554.

Easwaran, H.P., Leonhardt, H., and Cardoso, M.C. (2005). Cell cycle markers for live cell analyses. Cell Cycle 4, 453–455.

Essers, J., Theil, A.F., Baldeyron, C., van Cappellen, W.A., Houtsmuller, A.B., Kanaar, R., and Vermeulen, W. (2005). Nuclear dynamics of PCNA in DNA replication and repair. Mol. Cell. Biol. 25, 9350–9359.

Haubensak, W., Attardo, A., Denk, W., and Huttner, W.B. (2004). Neurons arise in the basal neuroepithelium of the early mammalian telencephalon: a major site of neurogenesis. Proc. Natl. Acad. Sci. USA 101, 3196–3201.

Hoffman, R.M. (2005). In vivo cell biology of cancer cells visualized with fluorescent proteins. Curr. Top. Dev. Biol. 70, 121–144.

Hoffman, R.M., and Yang, M. (2006). Whole-body imaging with fluorescent proteins. Nat. Protocols 3, 1429–1438.

Karasawa, S., Araki, T., Yamamoto-Hino, M., and Miyawaki, A. (2003). A green-emitting fluorescent protein from Galaxeidae coral and its monomeric version for use in fluorescent labeling. J. Biol. Chem. 278, 34167–34171.

Karasawa, S., Araki, T., Nagai, T., Mizuno, H., and Miyawaki, A. (2004). Cyan-emitting and orange-emitting fluorescent proteins as a donor/acceptor pair for fluorescence resonance energy transfer. Biochem. J. 381, 307–312.

Kisielewska, J., Lu, P., and Whitaker, M. (2005). GFP-PCNA as an S-phase marker in embryos during the first and subsequent cell cycles. Biol. Cell 97, 221–229.

Kogure, T., Karasawa, S., Araki, T., Saito, K., Kinjo, M., and Miyawaki, A. (2006). A fluorescent variant of a protein from the stony coral Montipora facilitates dual-color single-laser fluorescence cross-correlation spectroscopy. Nat. Biotechnol. 24, 577–581.

Lee, C., Hong, B.S., Choi, J.M., Kim, Y., Watanabe, S., Ishimi, Y., Enomoto, T., Tada, S., Kim, Y., and Cho, Y. (2004). Structual basis for inhibition of the replication licencing factor Cdt1 by geminin. Nature 430, 913–917.

Leonhardt, H., Rahn, H.P., Weinzierl, P., Sporbert, A., Cremer, T., Zink, D., and Cardoso, M.C. (2000). Dynamics of DNA replication factories in living cells. J. Cell Biol. 149, 271–279.

Marín, O., and Rubenstein, J.L.R. (2001). A long, remarkable journey: tangential migration in the telencephalon. Nat. Rev. Neurosci. 2, 780–790.

Miyata, T., Kawaguchi, A., Saito, K., Kuramochi, H., and Ogawa, M. (2002). Visualization of cell cycling by an improvement in slice culture methods. J. Neurosci. Res. 69, 861–868.

Miyata, T., Kawaguchi, A., Saito, K., Kawano, M., Muto, T., and Ogawa, M. (2004). Asymmetric production of surface-dividing and non-surface-dividing cortical progenitor cells. Development 131, 3133–3145.

Miyawaki, A., Llopis, J., Heim, R., McCaffery, J.M., Adams, J.A., Ikura, M., and Tsien, R.Y. (1997). Fluorescent indicators for Ca^{2+} based on green fluorescent protein and calmodulin. Nature 388, 882–887.

Miyoshi, H., Takahashi, M., Gage, F.H., and Verma, I.M. (1997). Stable and efficient gene transfer into the retina using an HIV-based lentiviral vector. Proc. Natl. Acad. Sci. USA 94, 10319–10323.

Miyoshi, H., Blömer, U., Takahashi, M., Gage, F.H., and Verma, I.M. (1998). Development of a self-inactivating lentivirus vector. J. Virol. 72, 8150–8157.

Mochizuki, N., Yamashita, S., Kurokawa, K., Ohba, Y., Nagai, T., Miyawaki, A., and Matsuda, M. (2001). Spatio-temporal images of growth-factor-induced activation of Ras and Rap1. Nature 411, 1065–1068.

Nakayama, K.I., and Nakayama, K. (2006). Ubiquitin ligases: cell-cycle control and cancer. Nat. Rev. Cancer 6, 369–381.

Neumann, C.J., and Nuesslein-Volhard, C. (2000). Patterning of the zebrafish retina by a wave of sonic hedgehog activity. Science 289, 2137–2139.

Nishitani, H., Lygerou, Z., Nishimoto, T., and Nurse, P. (2000). The Cdt1 protein is required to license DNA for replication in fission yeast. Nature 404, 625–628.

Nishitani, H., Lygerou, Z., and Nishimoto, T. (2004). Proteolysis of DNA replication licensing factor Cdt1 in S-phase is performed independently of geminin through its N-terminal region. J. Biol. Chem. 279, 30807–30816.

Nishitani, H., Sugimoto, N., Roukos, V., Nakanishi, Y., Saijo, M., Obuse, C., Tsurimoto, T., Nakayama, K.I., Nakayama, K., Fujita, M., et al. (2006). Two E3 ubiquitin ligases, SCF-Skp2 and DDB1-Cul4, target human Cdt1 for proteolysis. EMBO J. 25, 1126–1136.

Niwa, H., Yamamura, K., and Miyazaki, J. (1991). Efficient selection for high-expression transfectants with a novel eukaryotic vector. Gene 108, 193–199.

Noctor, S.C., Martinez-Cerdeno, V., Ivic, L., and Kriegstein, A.R. (2004). Cortical neurons arise in symmetric and asymmetric division zones and migrate through specific phases. Nat. Neurosci. 7, 136–144.

Nurse, P., Masui, Y., and Hartwell, L. (1998). Understanding the cell cycle. Nat. Med. 4, 1103–1106.

Nurse, P. (2000). A long twentieth century of the cell cycle and beyond. Cell 199, 71–78.

Piek, E., Moustakas, A., Kurisaki, A., Heldin, C.H., and Dijke, P. (1999). TGF-β type I receptor / ALK-5 and Smad proteins mediate epithelial to

mesenchymal transdifferentiation in NMuMG breast epithelial cells. J. Cell Sci. *112*, 4557–4568.

Sauer, F.C. (1935). Mitosis in the neural tube. J. Comp. Neurol. *62*, 377–405.

Senga, T., Sivaprasad, U., Zhu, W., Park, J.H., Arias, E.E., Walter, J.C., and Dutta, A. (2006). PCNA is a cofactor for Cdt1 degradation by CUL4/DDB1-mediated N-terminal ubiquitination. J. Biol. Chem. *281*, 6246–6252.

Shaner, N.C., Campbell, R.E., Steinbach, P.A., Giepmans, B.N., Palmer, A.E., and Tsien, R.Y. (2004). Improved monomeric red, orange and yellow fluorescent proteins derived from Discosoma sp. Red fluorescent protein. Nat. Biotechnol. *22*, 1567–1572.

Spella, M., Britz, O., Kotantaki, P., Lygerou, Z., Nishitani, H., Ramsay, R.G., Flordellis, C., Guillemot, F., Mantamadiotis, T., and Taraviras, S. (2007). Licensing regulators Geminin and Cdt1 identify progenitor cells of the mouse CNS in a specific phase of the cell cycle. Neuroscience *147*, 373–387.

Sugimoto, N., Tatsumi, Y., Tsurumi, T., Matsukage, A., Kiyono, T., Nishitani, H., and Fujita, M. (2004). Cdt1 phosphorylation by cyclin A-dependent kinases negatively regulates its function without affecting Geminin binding. J. Biol. Chem. *279*, 19691–19697.

Thiery, J.P., and Sleeman, J.P. (2006). Complex networks orchestrate epithelial-mesenchymal transitions. Nat. Rev. Mol. Cell Biol. *7*, 131–142.

Tojo, M., Hamashima, Y., Hanyu, A., Kajimoto, T., Saitoh, M., Miyazono, K., Noda, M., and Imamura, T. (2005). The ALK-5 inhibitor A-83–01 inhibits Smad signaling and epithelial-to-mesenchymal transition by transforming growth factor-β. Cancer Sci. *96*, 791–800.

Vaziri, C., Saxena, S., Jeon, Y., Lee, C., Murata, K., Machida, Y., Wagle, N., Su Hwang, D., and Dutta, A. (2003). A p53-dependent checkpoint pathway prevents rereplication. Mol. Cell *11*, 997–1008.

Vodermaier, H.C. (2004). APC/C and SCF: Controlling each other and the cell cycle. Curr. Biol. *14*, R787–R796.

Yamauchi, K., Yang, M., Jiang, P., Xu, M., Yamamoto, N., Tsuchiya, H., Tomita, K., Moossa, A.R., Bouvet, M., and Hoffman, R.M. (2006). Development of real-time subcellular dynamic multicolor imaging of cancer-cell trafficking in live mice with a variable-maginification whole-mouse imaging system. Cancer Res. *66*, 4208–4214.

Yang, M., Li, L., Jiamg, P., Moossa, A.R., Penman, S., and Hoffman, R.M. (2003). Dual-color fluorescence imaging distinguishes tumor cells from induced host angiogenic vessels and stromal cells. Proc. Natl. Acad. Sci. USA *100*, 14259–14262.

Yang, Y., Pan, X., Lei, W., Wang, J., and Song, J. (2006). Transforming growth factor-β1 induces epithelial-to-mesenchymal transition and apoptosis via a cell cycle-dependent mechanism. Oncogene *25*, 7235–7244.

Wei, W., Ayad, N.G., Wan, Y., Zhang, G.-J., Kirschner, M.W., and Kaelin, W.G., Jr. (2004). Degradation of the SCF component Skp2 in cell-cycle phase G1 by the anaphase-promoting complex. Nature *428*, 194–198.

Zetterberg, A., and Larsson, O. (1985). Kinetic analysis of regulatory events in G1 leading to proliferation of quiescence of Swiss3T3 cells. Proc. Natl. Acad. Sci. USA *82*, 5365–5369.

Zhang, G.-J., Safran, M., Wei, W., Sorensen, E., Lassota, P., Zhelev, N., Neuberg, D.S., Shapiro, G., and Kaelin, W.G., Jr. (2004). Bioluminescent imaging of Cdk2 inhibition in vivo. Nat. Med. *10*, 643–648.